Desalination and Water Treatment
www.deswater.com

doi: 10.5004/dwt.2020.25407

185 (2020) 209–225
May

Arsenic adsorption from groundwater using non-toxic waste as adsorbent

Dikshya Dhakal, Sandhya Babel*

School of Biochemical Engineering and Technology, Sirindhorn International Institute of Technology (SIIT), Thammasat University, Pathum Thani, Thailand, Tel. +662 986 9009 Ext. 2307; email: sandhya@siit.tu.ac.th (S. Babel), dikshya842@gmail.com (D. Dhakal)

Received 12 December 2018; Accepted 2 January 2020

ABSTRACT

Millions of people in the world are exposed to arsenic-contaminated groundwater. To decrease the concentration of arsenic in water, adsorption of arsenic was performed on a simple and easily available material, that is, eggshell. Powdered eggshell (ES) was prepared and was characterized by using Brunauer–Emmett–Teller, Fourier transform infrared spectroscopy (FTIR), scanning electron microscopy, and energy-dispersive X-ray spectroscopy (EDX). It was revealed from FTIR and EDX that the presence of $CaCO_3$ in ES is the major reason for arsenic adsorption. Removal of As(III) and As(V) as a function of the adsorbent dose, pH, contact time, and agitation speed were studied. The adsorption capacity is strongly influenced by the pH of the solution. ES removed 68.54% of As(III) and 72.01% of As(V) under optimum conditions from 2 mg/L As(III) and As(V) solutions. ES was also carbonized at 700°C, and it could remove 70.09% of As(III) and 76.44% of As(V) under similar conditions. Adsorption isotherms and kinetics were determined for As(III) and As(V). As(III) adsorption followed the Langmuir isotherm, revealing monolayer adsorption. As(V) adsorption followed the Freundlich isotherm, revealing multilayer adsorption. Similarly, adsorption of As(III) and As(V) on carbonized eggshell followed pseudo-second-order kinetics and on ES followed Elovich kinetics, both suggesting that the adsorption process is a chemisorption process. Also, the study of the intraparticle diffusion model concluded that there was surface adsorption along with an intraparticle diffusion mechanism during the adsorption of arsenic. The best isotherm and kinetic models were selected, based on the error values using the chi-square test, root mean square error, and average percentage error.

Keywords: Arsenite; Arsenate; Eggshell; Adsorption; Isotherm; Kinetics

1. Introduction

Rapid urbanization and population growth have triggered an increase in water consumption and wastewater generation. Households, institutions, and industries are disposing untreated wastewater carelessly. This causes severe deterioration of water bodies in the developing world. Huge quantities of wastewater are being disposed of in water bodies without proper treatment. This trend of disposal leads to the accumulation of harmful materials, including pathogens, toxic substances, biodegradable organic matter, and chemicals in streams and rivers. The ultimate consequences are a shortage of clean water and waterborne diseases. This obligates people to rely upon groundwater.

Groundwater is an important source of water for a wide range of purposes. Groundwater use has increased, as an alternative to polluted surface water. People in some regions depend upon groundwater for drinking and cooking purposes. However, groundwater is not a secure option. Groundwater contaminated with arsenic is a widespread environmental problem. Countries like Bangladesh and West Bengal (India) use groundwater as the main source of drinking water. However, the groundwater in these countries is severely contaminated with arsenic due to the release of arsenic from arsenic-contaminated sediments in

* Corresponding author.

groundwater aquifers and recharge areas [1]. Groundwater can also be contaminated through the infiltration of arsenic from contaminated soil. Arsenic accumulation in the soil may be attributed to the use of arsenical pesticides, application of fertilizers, mining activities, coal burning, smelter operations, and volcanic emissions. The accumulated arsenic can infiltrate water bodies after some time. Hence, the concentration of arsenic in water bodies is increasing day by day as a consequence of the growing industrialization and urbanization of the world.

At present, 70 countries are affected by water contaminated by arsenic [2]. About 150 million people around the world are affected by arsenic-contaminated water, among which 110 million people live in South and Southeast Asia [3]. Table 1 shows the concentration of arsenic in groundwater samples of different countries. WHO stated that the maximum concentration of arsenic that can be in drinking water (without causing any effects) is 10 μg/L [4]. Exposure to inorganic arsenic at lower levels can irritate the stomach and lungs. Exposure to higher levels may cause serious health hazards like infertility, miscarriages in women, and retarded development in children. It can affect the respiratory tract, cause cardiovascular abnormalities, gastrointestinal effects, brain damage, and even lower the immunity against some infections [5]. Long term exposure to a high arsenic concentration can cause diseases such as skin lesions and cancers that include hyper-pigmentation (excess skin pigmentation), hyperkeratosis, gangrene in a limb, skin cancer, lung cancer, and bladder cancer [6]. Arsenic also accumulates in the soil if the land is irrigated by water contaminated with arsenic. Once the soil is contaminated, this can decrease crop quality and crop yields. It is reported there was a 10% decrease in the rice yield due to the accumulation of arsenic in the soil at a concentration of 25 mg/kg [7]. Arsenic accumulation was due to irrigation with arsenic-contaminated water.

In natural water, inorganic arsenic is the predominant form, which exists in two oxidation states, arsenate [As(V)] and arsenite [As(III)] [14]. The most important parameters that control arsenic speciation are pH and redox potential. As(III) is highly toxic and mobile in comparison with As(V) [15]. To protect against the harmful effects of arsenic, treatment procedures must be applied prior to the usage of water. Coagulation and flocculation are the most common and widely used treatment processes, using iron (Fe) and aluminium (Al) based coagulants [16]. However, sludge containing arsenic is produced in large quantities which are difficult to manage. Membrane technology, ion exchange, oxidation, phytoremediation, and adsorption are other techniques that are used for the removal of arsenic. These technologies are either inefficient or expensive and complex for use at household level. A desirable technique is the adsorption technique due to its simple design, easy operation, and low investment in terms of initial cost and land area. Arsenic ions are strongly adsorbed on some of the minerals such as zeolite [17], siderite [18], hematite [19], etc. Industrial by-products, including fly ash [20], leather industry waste [20], slag from the steel industry [21], palm oil clinker [2], red mud [22], etc., were effective for the removal of arsenic. Agricultural and household wastes have also been investigated for arsenic removal. Copper modified coconut husk [23], iron-loaded wheat straw [24], orange peel activated by HCl [25], tea waste [1], fish scale [26], $FeCl_3$ treated lemon peel [14], $FeCl_3$ treated pomegranate peel [27], etc. significantly removed arsenic from aqueous solution. Although, various adsorbents have been studied for arsenic removal, there are only few studies that have determined the possibility of using biomass without any chemical treatment for arsenic removal.

Eggshells are significant solid waste, produced from poultry, homes, restaurants, bakeries, and food manufacturing units. An eggshell weighs about 10% of the total mass of a hen egg [28]. Eggshells and eggshell membranes show good efficiency in the removal of heavy metals, phenolic compounds, pesticides, and dyes because of their surface properties [29]. One gram of powdered eggshell contains about 22.4 mg of iron (Fe), 12.45 mg of aluminium (Al^{3+}), and 401 mg of calcium (Ca^{2+}) [30]. Iron and aluminium based coagulants have shown significant removal of arsenic in coagulation and flocculation processes [16]. Therefore, considering the composition of eggshell, it is believed that it has the potential to be employed for arsenic adsorption.

The present study investigates the efficiency of eggshell for the removal of As(III) and As(V). Batch experiments were carried out to find out the optimum adsorbent dose, pH, contact time, and agitation speed. Adsorption data were used to determine suitable isotherms and kinetic models. Some of the physical and chemical properties of eggshells were also studied.

2. Materials and methods

2.1. Materials

All stock solutions were prepared by using analytical reagent grade chemicals and distilled water. The stock solution of arsenite, As(III), was prepared from arsenic trioxide (As_2O_3) (Thermo Fisher Scientific, Singapore). As_2O_3 (1.320 g) was dissolved in 1,000 ml distilled water containing 4 g of NaOH, to prepare a stock solution of 1,000 mg/L [31]. The stock solution of arsenate, As(V), was prepared from 4.164 g of sodium heptahydrate ($Na_2HAsO_4{\cdot}7H_2O$) salt (≥98.0%, Sigma-Aldrich, Singapore). This was dissolved in 1 L to make a stock solution of 1,000 mg/L. Low concentration solutions were made from serial dilution. For pH adjustment, 0.1 N HCl (Lobal Chemie, Mumbai, India) and 0.1 N NaOH (Merck, Darmstad, Germany) solutions, were used.

Eggshells were collected from the food shop in SIIT, Thailand. The eggshells were first thoroughly washed with water to remove any exerting dirt. Then, they were washed with DI water, dried in an oven at 100°C until constant weight, ground to powder form, and sieved through a mesh sieve of 250 μm. The powdered eggshell (ES) was stored in an airtight container for further application. Thereafter, thermal activation was done by heating a powdered sample in a muffle furnace at 700°C ± 5°C for 5 h in contact with air. The resultant adsorbents were carbonized eggshell (CES). From 100 g of raw egg shell, 84.27 g of ES and 69.03 g of CES, were obtained.

2.2. Adsorbent characterization

ES and CES were characterized by different techniques to determine their physical and chemical properties.

The functional groups of ES and CES, before and after adsorption, were determined by infrared spectroscopy. FTIR measurements were carried out using a Nicolet iS50 FTIR spectrometer (Thermo Fisher Scientific, USA) by employing the KBr pellet method. Surface areas were obtained using a 3 Flex Version 3.02 (Micrometric, USA), according to the Brunauer–Emmett–Teller (BET) protocol. The surface morphology of the adsorbents (before and after) adsorption were studied using a field emission scanning electron microscope (JEOL, JSM-7800F, Japan), equipped with an energy dispersive X-ray fluorescence spectrometer (Oxford Instruments, X-Max^N, USA) that measures the elemental composition.

2.3. Optimization of influential parameters

The adsorption capacity of adsorbents depends on various experimental parameters such as adsorbent dose, pH of solution, time, etc. To determine suitable conditions for the removal of arsenic, experiments were performed on As(III) and As(V) solutions using ES. Once the optimum conditions were known, the removal capacity of CES was determined at those optimum conditions. According to Smedley and Kinniburgh [32], the maximum concentration of arsenic in groundwater is 2.5 mg/L in Bangladesh, 3.2 mg/L in West Bengal, 1.8 mg/L in Taiwan, 5.3 mg/L in Vietnam, 5.3 mg/L in Argentina, and 1.0 mg/L in northern Chile. Based on the range of these concentrations, as shown in Table 1, the initial concentration of arsenic was taken as 2 mg/l to carry out the experiments. For the experiments, a 2 mg/L arsenic solution was prepared from the stock solution by serial dilution. To observe the effects of adsorbent dose, 50 mL aliquots of the standard solutions were adjusted to pH 7, placed into conical flasks, and subjected to adsorbent doses of 2–10 g/L. The solutions were allowed to shake in a rotary shaker at 100 rpm for 2 h. Then, the solutions were filtered, and subsequent measurements were taken. The samples were filtered using nylon syringe filters of 0.22-micron pore size and 25 mm diameter. Arsenic was measured using an inductively coupled plasma-optical emission spectrometer (ICP-OES, Optima 8000, PerkinElmer, USA). The pH was measured using a portable pH meter (ST300, Ohaus Corporation, USA).

The arsenic uptake capacity of adsorbents depends upon a key parameter: pH of the solution. Therefore, the removal capacity of ES was observed at different pH levels, from 4 to 11. To study the surface charge of ES at different values of pH, the point of zero charge (pHpzc) was also determined. For that, 0.01 M NaCl solution was prepared, and 50 mL of the solution was taken and maintained at pH values of 2–11 (pH_i). ES (500 mg) was added to a conical flask and shaken at 120 rpm for 24 h to reach equilibrium. The final pH (pH_f) of the supernatant was measured, and pHpzc was determined. pHpzc is the point where the difference in the initial and final pH is zero ($\Delta pH = pH_i - pH_f = 0$).

The influence of contact time (40–240 min), agitation speed (50–250 rpm), and initial analyte concentration (0.1–10 mg/L), were also studied. Finally, the effects of presence of phosphate (PO_4^{3-}) and nitrate (NO_3^-) ions on arsenic removal efficiency were investigated. The concentration of arsenic and each anion were maintained at different ratios, using a constant arsenic concentration of 2 mg/L. The amount of adsorption at equilibrium is determined using Eq. (1). The removal percent (%) is calculated using Eq. (2):

$$q_e = \frac{V \times \left(C_i - C_e\right)}{M} \tag{1}$$

$$\text{Removal Percent} = \frac{C_i - C_e}{C_i} \times 100 \tag{2}$$

where, q_e: adsorption amount (mg/g); V: volume of solution (L); M: mass of adsorbent (g); C_i: initial arsenic concentration (mg/L); C_e: equilibrium arsenic concentration (mg/L).

2.4. Adsorption isotherms

Adsorption isotherms represent the equilibrium relationship that describes the interaction between adsorbate ions and the adsorbent's surface. Adsorption processes can take place by forming a homogeneous layer or a heterogeneous layer. Three isotherm models, namely, the Langmuir, Freundlich, and Elovich models were studied. These models are based on the assumption of the formation of either a homogeneous layer or a heterogeneous layer. Equilibrium experiments were performed, based on the optimum conditions obtained from the adsorption experiments: neutral pH and varying the arsenic concentration from 2 to 10 mg/L.

2.4.1. Langmuir adsorption isotherm

The Langmuir isotherm assumes that a fixed number of adsorption sites are present on the adsorbent's surface and all those vacant sites are of equal size and shape. Each vacant

Table 1
Arsenic concentration in groundwater of different countries

Location	Sampling time	Concentration (μg/L)	References
Nawalparasi, Nepal	2017	41.04–745.2	[8]
West Bengal, India	2003	1186 (maximum)	[9]
Punjab, Pakistan	2012	12–448.5	[10]
Jianghan Plain, China	May 2012–December 2013	0.71–1,081	[11]
Datong Basin, China (83 sample)	October 2016	0.31–452	[12]
Kushtia District, Bangladesh (49 sample)	September 2015	6.04–590	
Nakhon Si Thammarat province, Thailand	1996	1.25–5,114	[13]

site can hold one molecule, and a constant amount of heat is released in the process. The original non-linear and linear forms of the Langmuir adsorption isotherm used in this study are given in Eqs. (3) and (4), respectively.

$$q_e = \frac{Q_0 \mathrm{bC}_e}{1 + \mathrm{bC}_e} \tag{3}$$

$$\frac{C_e}{q_e} = \frac{1}{\mathrm{bQ}_0} + \frac{C_e}{Q_0} \tag{4}$$

where, C_e: equilibrium arsenic concentration (mg/L); q_e: amount of arsenic uptake per gram of adsorbent (mg/g); Q_0 and b are the Langmuir constants indicating the monolayer adsorption capacity (mg/g) and adsorption rate (L/mg), respectively. A graph was plotted between C_e/q_e and C_e, and the values of Q_0 and b were calculated from the graph. A dimensionless factor called the separation factor (R_L) that determines the nature of the adsorption process is determined using Eq. (5) [33].

$$R_L = \frac{1}{1 + \mathrm{bC}_i} \tag{5}$$

where, C_i: initial concentration of metal ions (mg/L).

2.4.2. Freundlich adsorption isotherm

Unlike the Langmuir isotherm model, the Freundlich isotherm model states that the adsorption process results in a heterogeneous adsorbate layer. According to the Freundlich isotherm, "the stronger binding sites are occupied first and adsorption energy decreases exponentially until the adsorption process completes" [33]. The non-linear equation and the logarithmic linear form of the Freundlich adsorption isotherm are given in Eqs. (6) and (7).

$$q_e = k_f C_e^{\frac{1}{n}} \tag{6}$$

$$\log q_e = \log k_f + \frac{1}{n} \log C_e \tag{7}$$

where, C_e: equilibrium arsenic concentration (mg/L); q_e: amount of arsenic adsorbed per gram of the adsorbent (mg/g); k_f and n: Freundlich constants that indicate the adsorption capacity and intensity, respectively. A graph was plotted between log q_e vs. log C_e. From the graph, the values of k_f and $1/n$ were calculated.

2.4.3. Elovich adsorption isotherm

The Elovich isotherm model is also based on the multilayer adsorption, as in the Freundlich isotherm model. The Elovich isotherm model assumes that the adsorption sites increase exponentially with adsorption, resulting in multilayer adsorption [34]. The Elovich isotherm model parameters are represented by Eq. (8) and the linearized form of the Elovich isotherm model is represented by Eq. (9) [34]:

$$\frac{q_e}{q_m} = K_e C_e \exp\left(-\frac{q_e}{q_m}\right) \tag{8}$$

$$\ln \frac{q_e}{q_m} = \ln K_e q_m - \frac{q_e}{q_m} \tag{9}$$

where, K_e: Elovich equilibrium constant (L/mg); q_m: Elovich maximum adsorption capacity (mg/g); C_e: equilibrium arsenic concentration (mg/L); q_e: adsorption capacity at equilibrium (mg/g). A graph is plotted for $\ln(q_e/C_e)$ vs. q_e and the values of q_m and K_e are then calculated from the graph.

2.5. Adsorption kinetics

In the adsorption process, the equilibrium time and rate of adsorption plays a significant role in controlling the process efficiency. Kinetic models, namely, pseudo-first-order, pseudo-second-order, Elovich equation, and Weber and Morris intraparticle diffusion models, were used in this study. Kinetic experiments were done using various contact time, optimum adsorbent dose, 2 mg/L initial analyte concentration, at pH 7.

2.5.1. Pseudo-first-order equation

The pseudo-first-order equation, also known as the Lagergren equation is probably the oldest empirical model to describe the rate of adsorption at the solid-liquid interface [35]. This model assumes that the rate of occupying sorption sites is proportional to the number of unoccupied sites [36]. The pseudo-first-order equation is derived using the Langmuir kinetic model. The integrated form of the Eq. (10) is as follows [34]:

$$\log\left(q_e - q_t\right) = \log q_e - \frac{k_1 t}{2.303} \tag{10}$$

where, k_1: pseudo-first-order rate coefficient (min^{-1}), q_e and q_t: Amount of arsenic adsorbed per gram of adsorbent at the equilibrium and at any time (mg/g), respectively. Values of k_1 and q_e were obtained from the curve between log (q_e–q_t) and t.

2.5.2. Pseudo-second-order equation

The pseudo-second-order kinetic model was proposed for divalent metal ions. This model is based on two assumptions. The first assumption is that two reactions occur simultaneously in the adsorption process. The second assumption is that one of the reactions occurs at a faster rate and reaches equilibrium quickly while the other reaction occurs at a slow rate and continues until the adsorption process is complete. The pseudo-second-order kinetic model's linearized form is represented as [37]:

$$\frac{t}{q_t} = \frac{1}{k_2 q_e^{\,2}} + \frac{1}{q_e} \times t \tag{11}$$

where, k_2: pseudo-second-order rate constant. Values of k_2 and q_e were obtained from the slope and intercept of the plot between t/q_t and t, respectively.

2.5.3. Elovich equation

The Elovich equation is used to describe the adsorption process, in which the adsorption rate decreases exponentially with an increase in the quantity of adsorbed ions [38]. If the adsorption process satisfies the Elovich equation, then it can be concluded that the adsorption process is a chemisorption process [34]. The Elovich Eq. (12) is generally represented by the following:

$$\frac{dq_t}{dt} = \alpha \exp\left(-\beta q_t\right) \tag{12}$$

where, q_t: adsorption capacity at time t (mg/g); α: initial sorption rate (mg/g min); β: desorption constant (g/mg). Chien and Clayton (1980) simplified the above equation with an assumption that the parameter $\alpha\beta >> 1$. So, integrating the equation at the boundary conditions, q_t (t = 0) = 0 and q_t (t = t) = q_t yields a simplified and linearized form of the Elovich equation as follows [34]:

$$q_t = \frac{1}{\beta}\ln\left(\alpha\beta\right) + \frac{1}{\beta}\ln\left(t\right) \tag{13}$$

A graph is plotted between q_t and ln(t), and the values of α and β are calculated. The higher the value of α, the greater is the adsorption rate compared with the desorption rate.

2.5.4. Weber and Morris intraparticle diffusion model

The Weber and Morris intraparticle diffusion model is used to identify the diffusion mechanism during the transportation of adsorbate from the solution to the particle surface. It states that "the solute uptake is proportional to the square root of time" [39]. The Eq. (14) for this model is the following:

$$q_t = k_{\text{int}} \times t^{1/2} + c \tag{14}$$

where, q_t: adsorption capacity at time t (mg/g); k_{int}: intraparticle diffusion rate constant (mgg^{-1}min$^{-0.5}$). Values of k_{int} and c were obtained from the slope and intercept, respectively, of a plot between q_t and $t^{1/2}$.

2.6. Analysis of best-fitting isotherm model and kinetics

A common procedure to select and compare models is by a comparison of the R^2 values. However, it is not always appropriate to evaluate the goodness of fit of a model, based on the R^2 value, especially when the data points undergo linear transformations [40]. To investigate the suitable models that represent arsenic adsorption on the adsorbents, some statistical analysis tools were applied. The R^2 value represents how close the data are fitted to the regression line but error analysis tools give the difference between the exact value and the model value. Once we get the isotherm constant values from the model, the values were substituted in the original non-linearized equation for the isotherm model and in the linearized equation for the kinetic model. Finally, adsorption capacity values were calculated from the model equations. The error between the calculated and the experimental values were obtained using three error analysis tools that are given below.

- *Chi-square test (χ^2)*: The chi-square test is given in Eq. (15) [34].
- *Root mean square error (RMSE)*: The RMSE test is given in Eq. (16) [34].
- *Average percentage error (APE)*: This is expressed in terms of percentage and is given in Eq. (17) [34].

$$\chi^2 = \sum_{i=1}^{N} \frac{\left(q_{e,\text{exp},i} - q_{e,\text{cal},i}\right)^2}{q_{e,\text{exp},i}} \tag{15}$$

$$\text{RMSE} = \sqrt{\frac{\sum_{i=1}^{N}\left(q_{e,\text{cal},i} - q_{e,\text{exp},i}\right)^2}{N}} \tag{16}$$

$$\text{APE}\left(\%\right) = \frac{\sum_{i=1}^{N}\left|\frac{q_{e,\text{exp},i} - q_{e,\text{cal},i}}{q_{e,\text{exp},i}}\right|}{N} \times 100 \tag{17}$$

where, $q_{e,\text{exp}}$: adsorption capacity obtained from the experiment (mg/g); $q_{e,\text{cal}}$: adsorption capacity obtained from theoretical calculation from the model (mg/g); N: number of observations. The lower the value of the error, the better is the model.

3. Results and discussion

3.1. Adsorbent characterization

3.1.1. Surface area and pore volume

The main physical parameter that is related to the efficiency of the adsorbent to adsorb metal ions is its surface area. The BET surface areas of ES and CES were 0.78 and 0.44 m^2/g, respectively, with a pore diameter of 7.76 and 6.32 nm. BET plots of ES and CES are given in Fig. 1. The pore diameter of ES and CES lies in the range of 2–50 nm. Hence, the pores are classified as mesopores [41]. The adsorbed molecule first gets settled in the macropores, followed by mesopores and micropores. The total pore volume of ES and CES were found to be 0.00263 and 0.0013 cm^3/g, respectively. The BET surface area depends on the degassing process and temperature. The process involved in degassing the sample is very complex and may result in a low surface area [42]. Some minerals used for arsenic removal, such as zeolite and hematite, had a high surface area of 450 and 50 m^2/g, respectively [17,19]. However, some biomass, such as tea waste and pomegranate peel, had a low surface area of 0.79 and 1.28 m^2/g, respectively, and showed significant arsenic adsorption [20,42]. The surface area is a factor that is responsible for adsorption, and functional groups also play a key role. Thus, these adsorbents were analyzed using Fourier transform infrared spectroscopy (FTIR).

3.1.2. Fourier transform infrared spectroscopy

Functional groups of adsorbents are one of the major factors that affect the process of adsorption. To understand

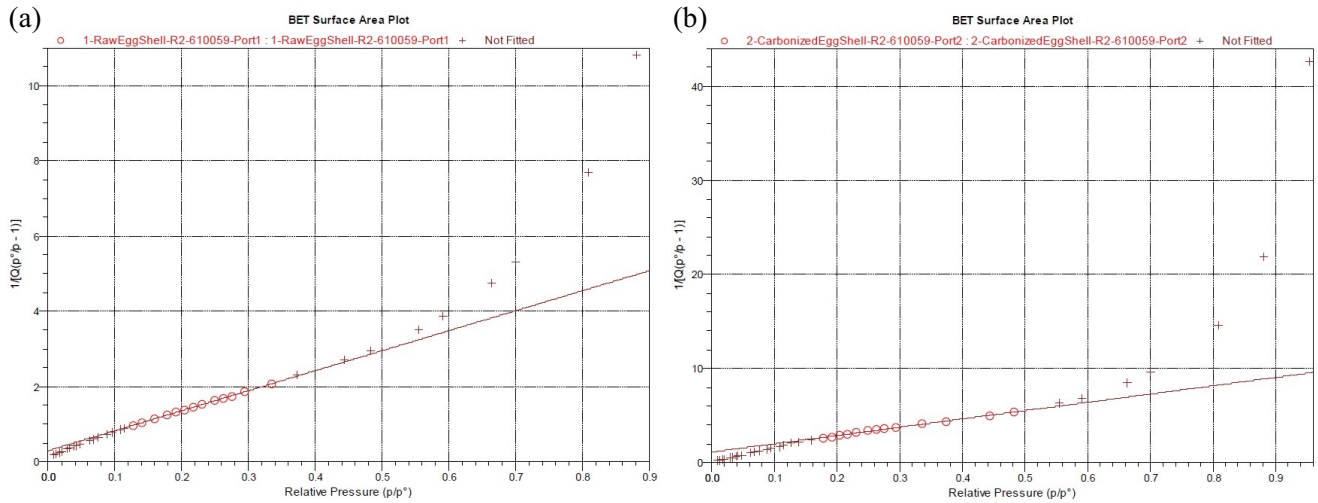

Fig. 1. BET surface area plot of (a) ES and (b) CES.

the functional groups present in the adsorbents, the FTIR spectra of ES and CES were obtained. The spectra of ES in Fig. 2a shows that the most significant peak occurs at a wavenumber of about 1,424 cm^{-1}, which is the characteristic peak of the carbonate (CO_3^-) group. This indicates that eggshell has the carbonate (CO_3^-) group. Peaks at a wavenumber of about 875 and 712 cm^{-1} could also be seen in the spectra. Those peaks are related to the out-of-plane deformation mode and in-plane deformation mode, respectively, indicating the presence of calcium carbonate [43]. The broad band appearing at 3,000 to 3,600 cm^{-1} corresponds to the presence of amines and amides (N–H stretching), found in protein fibers of the eggshell particles. Bending vibration in primary amines resulted in a peak corresponding to 1,795 cm^{-1} [44]. The peak at 2,509 cm^{-1} is attributed to vibrations of the C–O bond in CO_2 molecules, which exist in the air at ambient temperature and could be adsorbed on the surface of a sample [45]. CES also has this peak at the same wavenumber as ES, as shown in Fig. 2b.

Arsenic adsorption experiments were done by using ES and CES. FTIR spectra of those arsenic ion loaded adsorbents were obtained to see the changes in the original sample. Fig. 2 shows the FTIR spectra of adsorbents before and after adsorption. It was observed that the peak at 1,424 cm^{-1} decreased on the spectra of arsenic-loaded adsorbents. There is a decrease in the absorbance value of the three peaks at 1,424; 874, and 711 cm^{-1}. All these peaks are associated with the presence of calcium carbonate. This decrease in the band intensity revealed the substantial contribution of the calcium carbonate group in arsenic adsorption.

3.1.3. Scanning electron microscopy

The surface morphology of adsorbents before and after adsorption was seen using SEM analysis. SEM images before and after adsorption revealed that significant changes occurred on the surface of adsorbents due to adsorption. It can be seen in Fig. 3 that adsorbents before adsorption exhibit a flat and uniform surface while arsenic-loaded adsorbents exhibit particles cluttered on the adsorbent surface. Before adsorption, the adsorbent surface was smooth, which drastically changed into irregular, uneven, and rough surfaces. These changes, seen in the adsorbent surface from homogeneous layer to heterogeneous layer, could be due to the adsorption of arsenic. SEM images revealed that the adsorbents are composed of flat-shaped particles. This is also one reason for the lower surface area of the adsorbents, as shown by BET surface area analysis. Some pores are seen at the surface of the CES. These pores may be the result of the release of volatile gases or decomposition of organic compounds during the process of carbonization [46].

3.1.4. Energy-dispersive X-ray spectroscopy

Energy-dispersive X-ray spectroscopy (EDX) analysis was done to get information about the chemical composition of the adsorbents, before and after adsorption. ES and CES revealed the presence of C, O, Mg, and Ca, as shown in Table 2. ES also had an additional element, that is, Na. In a comparison of the elemental weight before and after adsorption, the weight percentage of C and O decreased while that of Ca increased. This can be attributed to the ion exchange mechanism during adsorption [36]. ES and CES consist of $CaCO_3$ as a chemical compound. During the process of adsorption, Ca adsorb arsenic ion and CO_3 is released into the solution. The decrease in carbonate groups is shown by FTIR analysis in Fig. 2. However, arsenic was not observed due to the lower adsorption capacity of the adsorbents. Iqbal and Saeed also showed the disappearance of Ca and K ion after lead adsorption due to the involvement of these ions in the ion exchange mechanism [36]. The changes in the elemental weight of Mg, Ca, and Na demonstrate some changes in the adsorbent that are due to the adsorption of arsenic.

3.2. Optimization of influential parameters

3.2.1. Adsorbent dose

The adsorption of arsenic by ES from 2 mg/L arsenic solution as a function of the adsorbent dose is plotted, as

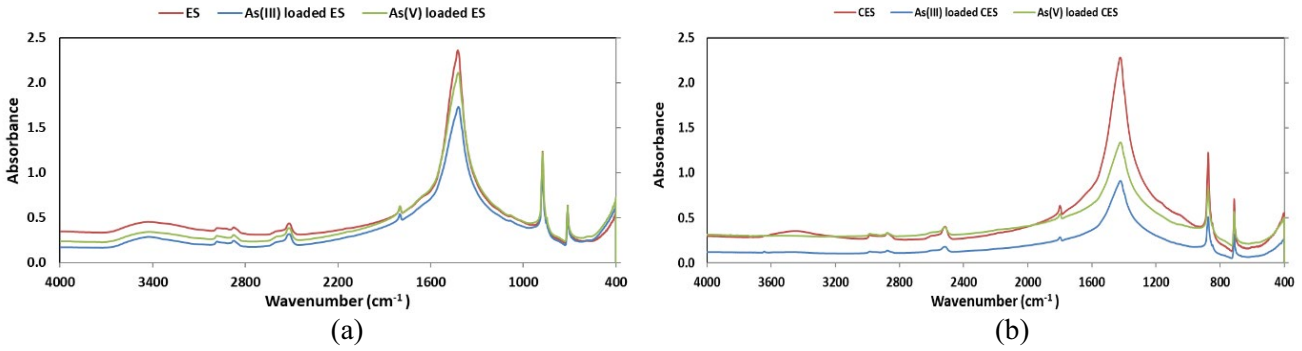

Fig. 2. FTIR spectra of (a) ES, As(III) loaded ES, and As(V) loaded ES (b) CES, As(III) loaded CES, and As(V) loaded CES.

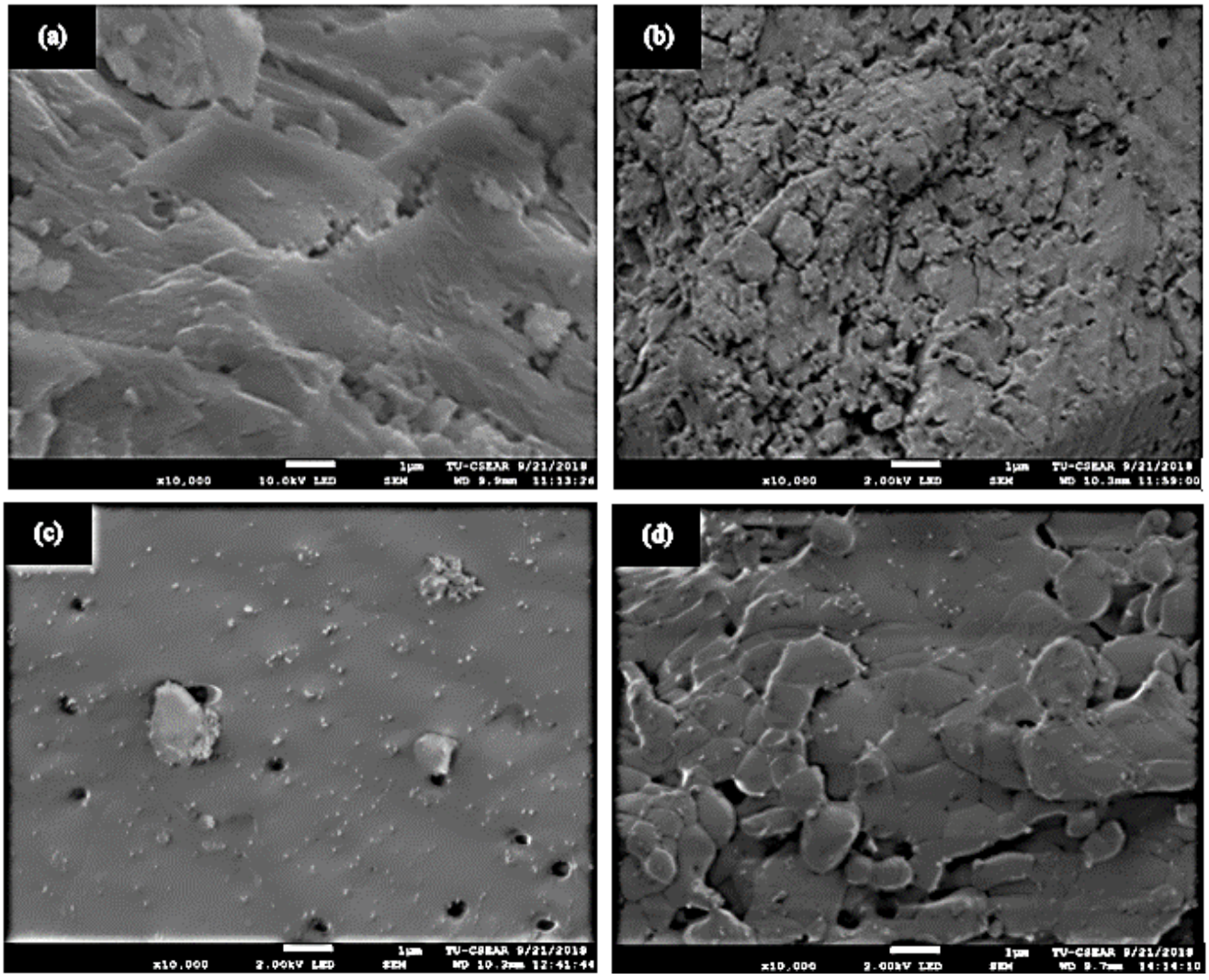

Fig. 3. SEM images of (a) ES, (b) ES after adsorption, (c) CES, and (d) CES after adsorption (10,000X).

shown in Fig. 4. The experimental observation, within the range of this study indicated that an increased adsorbent dose increased the removal percentage. As(III) and As(V) removal efficiency increased from 34% to 62% and 54% to 65%, respectively, when the adsorbent dose was increased from 2 to10 g/L of ES. As the quantity of adsorbent increases, the total surface area and the number of active sites for adsorption also increase, with enhanced adsorption. However, a significant change in removal was not observed beyond an adsorbent dose of 6 g/L due to the overlapping of binding sites. Hence,

Table 2
Elemental composition of ES and CES before and after adsorption by EDX

Element weight (%)	ES before adsorption	ES after adsorption	CES before adsorption	CES after adsorption
C	16.38	8.97	14.42	10.51
O	55.01	34.83	58.00	53.52
Mg	0.44	–	0.54	0.34
Ca	28.04	56.20	27.05	30.63
Na	0.13	–	–	–

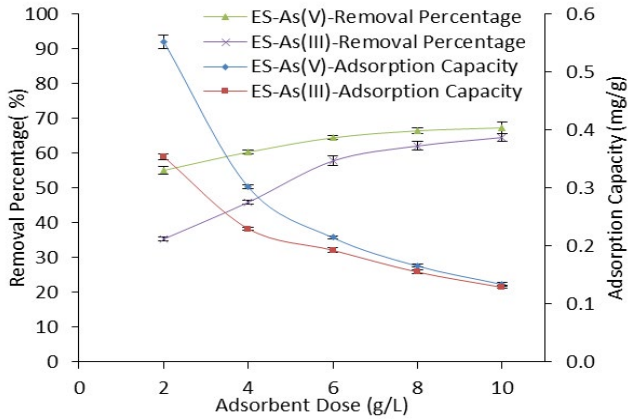

Fig. 4. Effects of adsorbent dose on the removal of As(III) and As(V) by using ES (experimental conditions: pH: 7; time: 2 h; speed: 100 rpm).

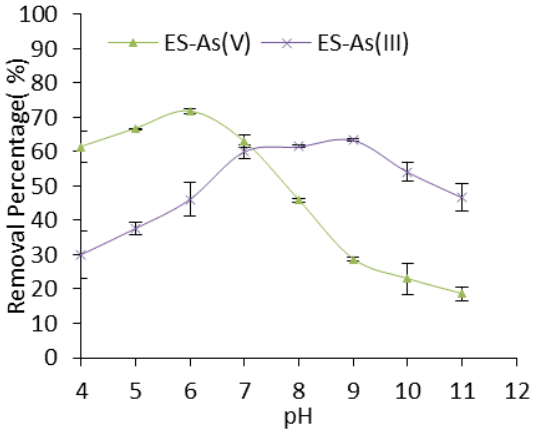

Fig. 5. Effects of pH on the removal of As(III) and As(V) by using ES (time: 2 h; speed: 100 rpm).

6 g/L was used as the optimum dose for further experiments. The actual mechanism for the removal of arsenic by eggshell is due to the presence of $CaCO_3$, which is described by the following Eq. (18) [47].

$$HAsO_3^{2-} + Ca^{2+} + nH_2O \rightarrow CaHAsO_3.nH_2O \quad (18)$$

3.2.2. pH

Fig. 5 shows the effects of pH variation on adsorption with an optimum dose of 6 g/L. As the pH increased, As (III) removal efficiency increased and reached a maximum value of 63.37% at pH 9. At lower pH, the concentration of H^+ ion is high, and adsorbents adsorb H^+ ions over metal ions [48]. The $H_2AsO_3^-$ state of arsenite starts to appear and increases from pH 7. This led to the adsorption of arsenic ions and became maximum at pH 9. When the pH is greater than 9, As (III) exists in the anion form as $H_2AsO_3^-$ and $HAsO_3^{2-}$ [15]. As the pH reaches the maximum value, the form of arsenic becomes more negatively charged, as AsO_3^{3-}. Moreover, at high pH values, the surface of adsorbents also becomes negatively charged [49]. Hence. the negatively charged species have higher electrostatic repulsion with the adsorbents, which weakens the adsorption capacity. This resulted in a decrease in adsorption capacity at higher pH. Similar results were obtained for iron-modified bamboo charcoal for arsenite adsorption [49]. For eggshell containing calcium carbonate, the following reaction occurs between arsenite and calcium ions from pH 9 to 11 [22].

$$2H_2AsO_3^- + Ca^{2+} + nH_2O \rightarrow Ca(H_2AsO_3)_2.nH_2O \quad (19)$$

For As(V), there was higher adsorption (71.77%) at pH 6, and the adsorption capacity decreased continuously as the pH increased. As(V) exists in the form of oxyanions ($H_2AsO_4^-$ and $HAsO_4^{2-}$) at neutral pH, and $H_2AsO_4^-$ is present at a lower value of pH [15]. As(V) species remain in the form of anions regardless of the pH of the solution. However, as the pH increases, the adsorbent surface gains more negativity which enhances the electrostatic repulsion among the adsorbent surface and the negatively charged As(V) species [49]. Arsenate ions and calcium ions present on eggshell react at pH 2–7 [22]. The chemical reaction is as follows:

$$2H_2AsO_3^- + Ca^{2+} + nH_2O \rightarrow Ca(H_2AsO_4)_2.nH_2O \quad (20)$$

Hence, As(V) adsorption favors a lower pH. Additionally, the removal efficiency at neutral pH is favorable for both states of arsenic. This suggests a practical application of these adsorbents to treat groundwater. For further experiments, the As(III) solution was adjusted to pH 9, and the As(V) solution was adjusted to pH 6.

To understand the influence of pH on adsorption more clearly, it is necessary to determine the point of zero charge of adsorbents. For that, the difference in the initial and final pH (ΔpH) vs. initial pH was plotted in a graph, as shown in Fig. 6. The point of zero charge is the point where, ΔpH = 0 and was found to be at pH 8.03 for ES. The surface of the

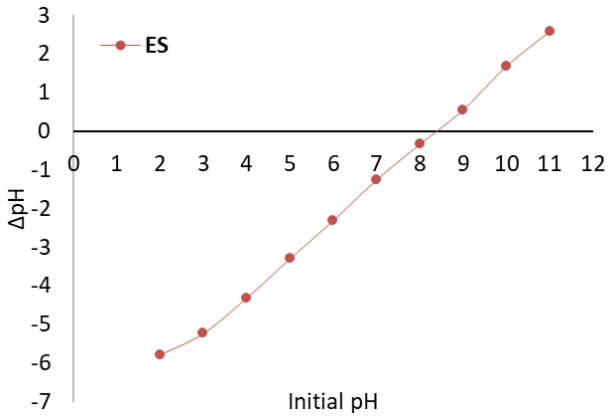

Fig. 6. Point of zero charge (pHpzc) curve of ES.

adsorbent is positive at pH below pHpzc and is negative at pH above pHpzc [50]. Therefore, pH below pHpzc is favorable for anions while pH above pHpzc is favorable for cations. Arsenate ions remain in the form of oxyanions throughout the pH range, and hence, adsorption is favored at pH below pHpzc. There is an electrostatic attraction between the arsenate ions and positively charged adsorbent's surface during the adsorption process. Arsenite ions stayed in protonated form until pH 7, so pH below pHpzc was not favorable for adsorption.

3.2.3. Contact time

The adsorption capacity was also optimized with respect to retention time. Fig. 7 shows the variation in As(III) and As(V) adsorption capacity with a change in retention time. The results revealed that as the retention time increased, the adsorption capacity of the adsorbents increased and gradually was constant after a certain period of time. This is because, at the initial phase, more vacant sites are present for adsorption but as time passes by, the vacant sites are occupied and no further adsorption takes place. The constant removal percentages after 160 min for As(III) and 80 min for As(V) suggest an equilibrium time. Hence, 160 min for As(III) and 80 min for As(V) is taken as the optimum time, which is enough for ES to adsorb arsenic ions. Consequently, further experiments were done using this equilibrium time.

3.2.4. Agitation speed

Optimum agitation speed should be determined to prevent either agglomeration of the adsorbents at the bottom due to low speed or to prevent the dissolving of adsorbents due to rapid speed. The effects of agitation speed are plotted in Fig. 8. The agitation speed does not significantly affect the removal efficiency of arsenic species.

3.2.5. Initial analyte concentration

There was a slight improvement in the removal efficiency when the initial analyte concentration decreased. As the initial analyte concentration decreased from 2 to 0.1 mg/L, an increase in the removal capacity was seen by almost 9% and 12% for As(III) and As(V) removal, respectively. Conversely,

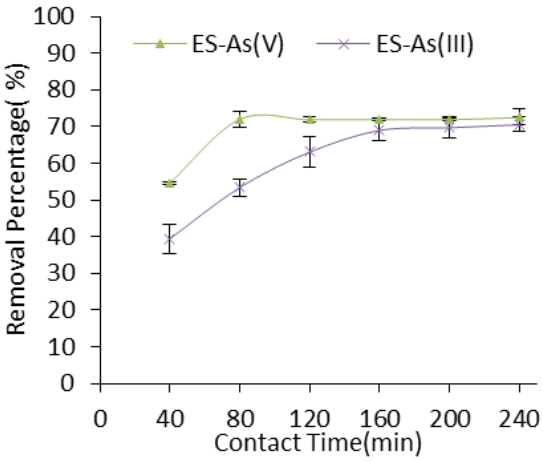

Fig. 7. Effects of contact time on the removal of As(III) and As(V) by using ES (Speed: 100 rpm).

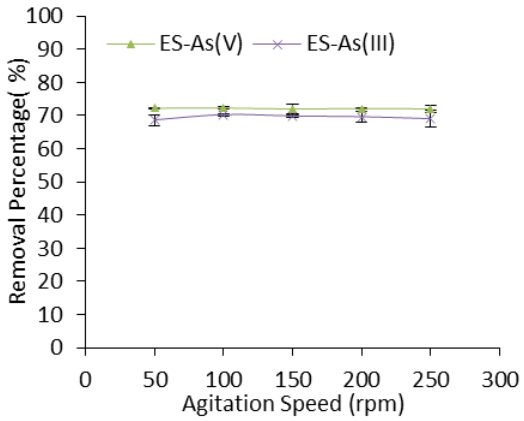

Fig. 8. Effects of agitation speed on the removal of As(III) and As(V) by using ES.

the removal percentage decreased with increased analyte concentration. As shown in Fig. 9, increasing the arsenic concentration five-fold, decreased the removal efficiency by about 35% and 28% for As(III) and As(V) removal, respectively. For the same adsorbent dose, the active sites present on the adsorbent surface are effective in removing the metal ions from low concentration solutions. However, as the concentration increases, the sites are filled and saturation is attained. This leads to an increased concentration in the solution itself, which results in a lowered removal efficiency. However, there was a continuous increase in arsenic adsorption capacity with the same adsorbent dose, as shown in Fig. 9. The increased adsorption capacity is due to the presence of a large number of arsenic ions in the solution at a higher concentration that causes greater interactions between adsorbent and ions [49].

3.2.6. Co-existing ions

Fig. 10 shows the efficiency of ES to remove As(III) and As(V) in the presence of competing solutes, including phosphate and nitrate. It can be seen that phosphate and

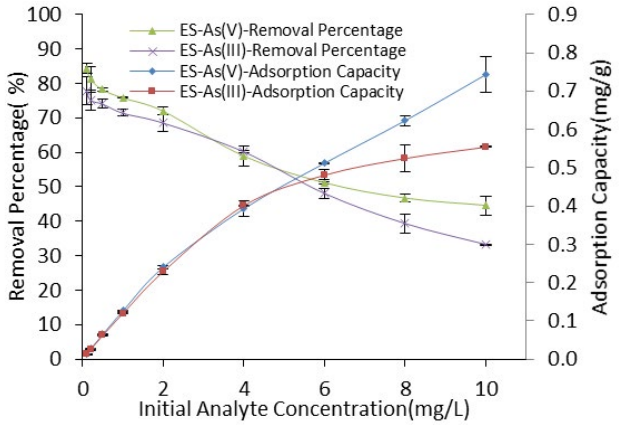

Fig. 9. Effects of initial analyte concentration on removal of As(III) and As(V) by using ES.

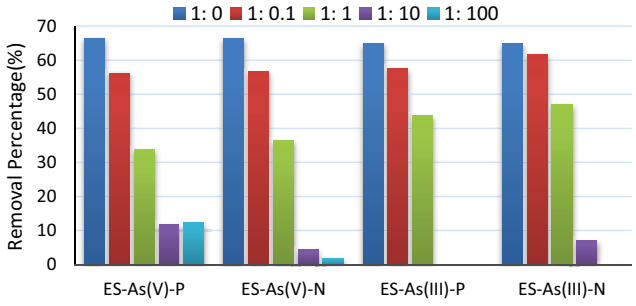

Fig. 10. Amount of arsenic removed in the presence of Phosphate (P) and Nitrate (N) ions at different ratios by using ES (At optimum conditions with initial arsenic concentration of 2 mg/L at pH 7).

nitrate ions have a significant influence on arsenic removal efficiency at pH 7. Results indicated that arsenic ions and these ions compete to be adsorbed on the adsorbent surface, decreasing arsenic removal efficiency. The adsorbent surface shows a higher affinity for competing ions than arsenic ions. As the concentration of co-existing ions increases, arsenic removal efficiency decreases and even becomes zero in the case of As(III) adsorption. When the ratio of arsenic ions and competing ions is 1:0.1, the results are slightly affected but as soon as the concentration increases, the removal efficiency significantly decreased. Phosphate ions show a higher affinity for the adsorbent surface even at a low concentration and compete with arsenic ions for binding sites, as arsenic ions and phosphate ions are similar in structure [51]. Jeong et al. [51] and Kanel et al. [52] also showed a sharp decrease in As(V) and As(III) removal efficiency with the addition of phosphate ions but no such effect was reported in removal efficiency with the addition of nitrate. The effects of co-existing ions depend on the pH of the solution and the functional groups present in the adsorbent. In this study, nitrate ions and phosphate ions equally affected the removal efficiency.

3.2.7. Adsorption by CES

From the experiments to optimize the influential parameters, the optimum conditions were found to be 6 g/L of adsorbent dose, pH 6 for As(III) and pH 9 for As(V) removal, and contact time of 160 min for As(III) and 80 min for As(V) removal. These conditions were applied for As(III) and As(V) removal using CES, and a graph is shown in Fig. 11. The removal efficiency of CES for As(III) removal is 72.04% and for As(V) removal is 77.29% from 2 mg/L arsenic solution. Similarly, the adsorption capacity to adsorb As(III) ions is 0.24 mg/g and to adsorb As(V) ions is 0.26 mg/g from 2 mg/L arsenic solution. The efficiency is improved a little by carbonization.

3.3. Adsorption isotherms

The adsorption parameters for each model were determined using the linear form of the equations. Fig. 12 shows graphs obtained for different isotherm models. The constant values calculated from the isotherm graphs, R^2 values, and error values calculated from error functions are listed in Table 3.

A comparison is made among the three isotherm models, based on the R^2 and error values that are listed in Table 3. A higher correlation coefficient (R^2) value for As(III) adsorption on ES and CES was observed in the Langmuir isotherm than the Freundlich and Elovich isotherms. Similarly, based on the R^2 value, As(V) adsorption on ES fits the Freundlich isotherm model while CES fits the Langmuir isotherm model. Further verification of the goodness of fit of a model was done using three different error analysis tools, as described before.

The results from error analysis yielded that the error values are in accordance with the R^2 values for As(III) adsorption. As(III) adsorption showed the greatest fit to the Langmuir model, with the least error values and high R^2 values. This reveals that monolayer adsorption is taking place between As(III) ions and adsorbents. In addition, there is a linear relationship between the equilibrium concentration and the ratio of the equilibrium concentration to adsorption capacity for As(III) adsorption. Furthermore, the highest value of b, in the case of As(III) adsorption on ES, signifies stronger bonds between As(III) ions and eggshell than with other adsorbents.

For As(V) adsorption, lower error values were obtained for the Freundlich isotherm model, followed by the

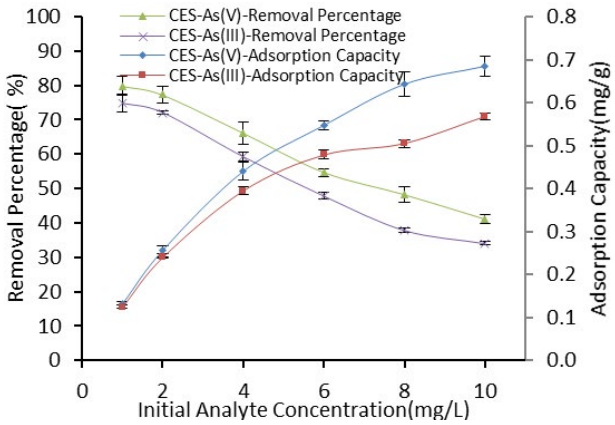

Fig. 11. As(III) and As(V) removal by using CES at different initial analyte concentrations.

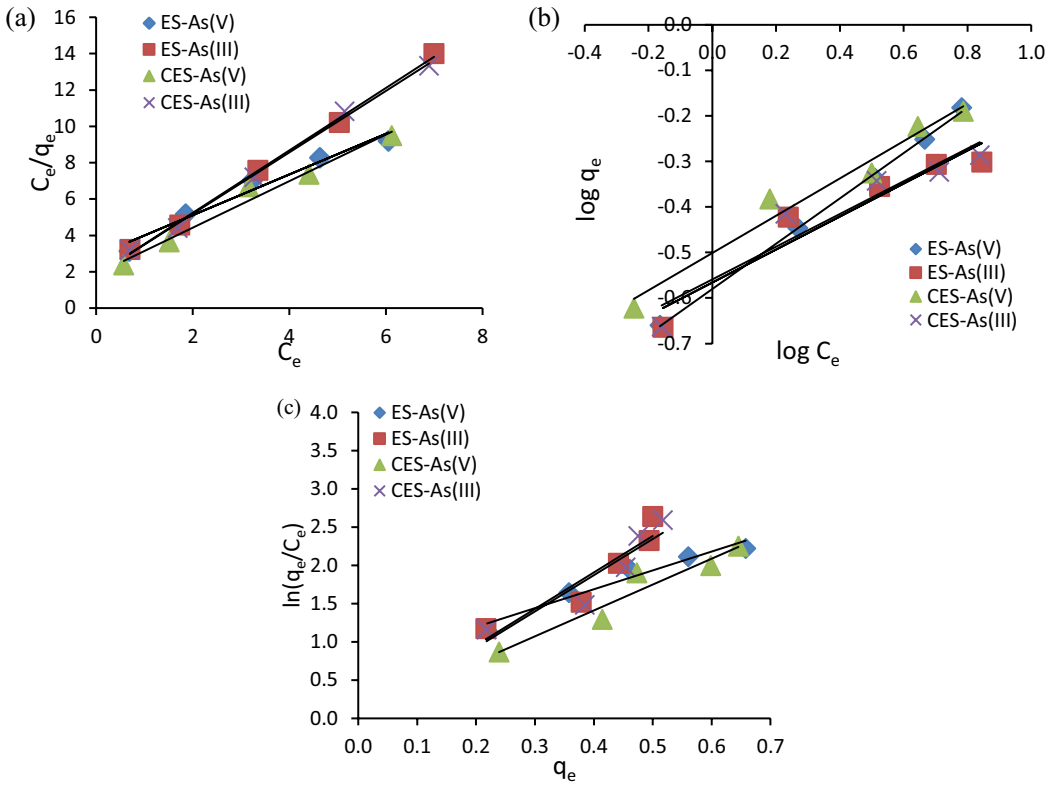

Fig. 12. (a) Langmuir, (b) Freundlich, and (c) Elovich adsorption isotherms of As(III) and As(V) adsorption by ES and CES (Adsorbent dose: 6 g/L; pH: 7, contact time: 80 min for As(III) and 160 min for As(V); speed: 100 rpm).

Table 3
Isotherm constant of three models with error analysis values

Adsorption Isotherm	Parameters	Adsorbent for As(III)		Adsorbent for As(V)	
		ES	CES	ES	CES
Langmuir	b (L/mg)	0.955	0.933	0.390	0.649
	Q_0 (mg/g)	0.581	0.591	0.892	0.793
	R^2	**0.997**	**0.996**	0.964	**0.988**
	χ^2	**0.002**	**0.003**	0.010	0.011
	RMSE	**0.012**	**0.014**	0.028	0.032
	APE (%)	**3.139**	**3.736**	6.784	6.430
Freundlich	k_f	0.269	0.275	0.263	0.316
	$1/n$	0.360	0.360	0.500	0.410
	n	2.780	2.780	2.000	2.440
	(R^2)	0.919	0.910	**0.998**	0.969
	χ^2	0.015	0.016	**0.001**	**0.009**
	RMSE	0.033	0.035	**0.008**	**0.027**
	APE (%)	7.886	8.512	**1.206**	**5.088**
Elovich	q_m	4.760	4.730	2.470	3.330
	K_e	0.002	–0.020	0.700	0.090
	R^2	0.877	0.862	0.949	0.978
	χ^2	26.885	N/A	6.455	0.288
	RMSE	0.382	N/A	1.761	0.164
	APE (%)	92.516	N/A	355.447	32.472

Highest R^2 value and the lowest χ^2, RMSE, and APE (%) values among the three isotherm models are in bold. N/A: Not Analyzed

Langmuir and Elovich models. The results are opposite to the R^2 values for As(V) adsorption on CES. This shows that it is not always appropriate to evaluate the goodness of fit of a model, based on the R^2 value. However, it is clear from the error values that As(V) adsorption on ES and CES best fits the Freundlich isotherm model, suggesting that the adsorption of As(V) occurs in multilayers. The value of n (Freundlich constant) describes the adsorption process. As shown in Table 3, the values of n are 2–10 and represent good adsorption [53]. Similarly, a higher value of $1/n$, in the case of As(V) adsorption on ES, indicates that the removal of As(V) using ES is more favorable than other cases [54].

A dimensionless factor called the separation factor (R_L) is used to determine the nature of an adsorption process. R_L values of different adsorbents at different concentrations are listed in Table 4. The value of R_L indicates the adsorption nature to be unfavorable ($R_L > 1$), linear ($R_L = 1$), favorable ($0 < R_L < 1$), or irreversible ($R_L = 0$) [33]. The lower the value of R_L, the more favorable is the adsorption process. All the values of R_L listed in Table 4 are in a range of 0–1 for an analyte concentration of 2–10 mg/L. This shows that the arsenic adsorption process is favorable for ES and CES under the specified optimum conditions.

3.4. Adsorption kinetics

To understand the adsorption process and the factors affecting the adsorption process, four kinetic models were studied: pseudo-first-order, pseudo-second-order, Elovich model, and Weber and Morris intraparticle diffusion models. The graphs, obtained for different kinetic models, are shown in Fig. 13. The constant values of the kinetic equations

Table 4
Separation factor (R_L) of different adsorbents at different analyte concentrations

Initial arsenic concentration	R_L values			
	ES-As(III)	CES-As(III)	ES-As(V)	CES-As(V)
2	0.344	0.349	0.562	0.435
4	0.207	0.211	0.391	0.278
6	0.149	0.152	0.299	0.204
8	0.116	0.118	0.243	0.161
10	0.095	0.097	0.204	0.134

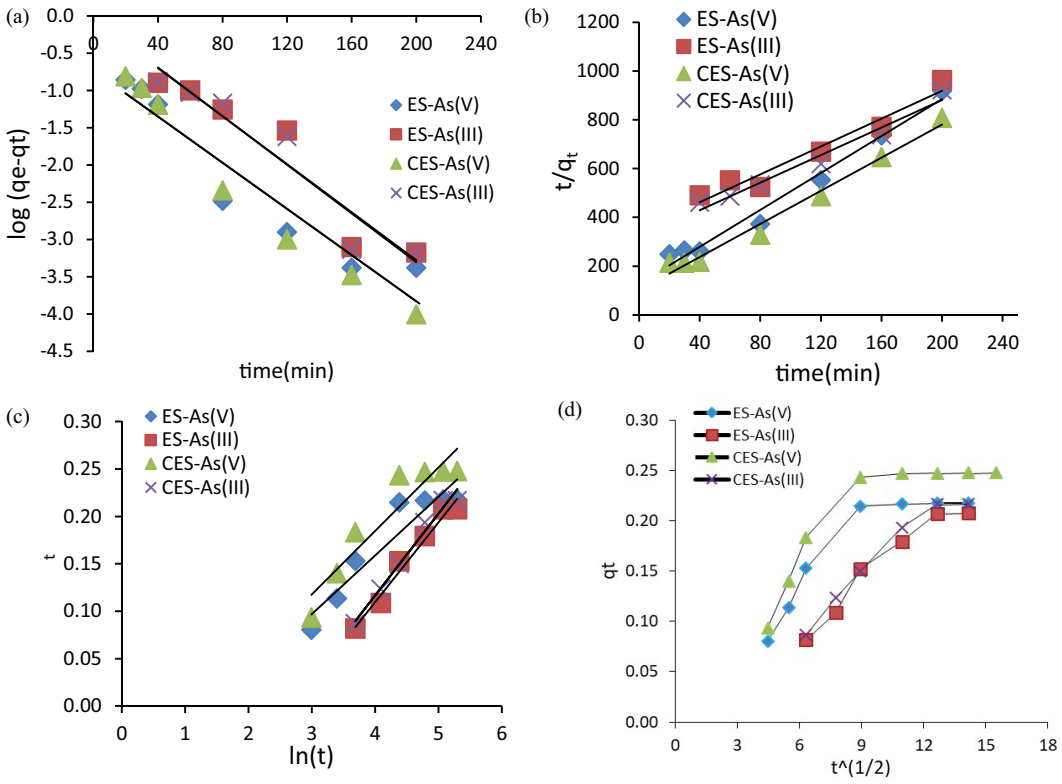

Fig. 13. (a) Pseudo-first-order, (b) pseudo-second-order, (c) Elovich kinetics, and (d) Weber and Morris intraparticle diffusion models of adsorption of As(III) and As(V) by ES and CES (Adsorbent dose: 6 g/L; pH: 7; initial analyte concentration: 2 mg/L; speed: 100 rpm).

calculated from the graph, R^2 values, and error values calculated from error functions are listed in Table 5.

Obtaining the kinetics parameters by linear regression shows that As(III) adsorption fits the Elovich kinetic equation and As(V) adsorption fits the pseudo-second-order kinetic equation, with respect to the R^2 values. But as mentioned before, linearization may result in some bias, and thus, error analysis tools were applied to select a suitable kinetic model. Each error value showed a clear result for As(V) adsorption. The least error values were obtained for the Elovich equation and the pseudo-second-order kinetic equation for As(V) adsorption on ES and CES, respectively. However, the error analysis tools did not give a consistent result for As(III) adsorption, and an overall optimum model was difficult to identify. In such cases, normalization and a combination of error values for each set are done, for a better comparison of the different errors. The error value obtained from each error function for each model was divided by the largest error value for that set of error functions. After that, the normalized error value of each kinetic model was combined, and are listed as the summation of the normalized error (SNE) in Table 5. Based on the SNE, the adsorption of As(III) and As(V) on ES follows the Elovich kinetic equation while the adsorption of As(III) and As(V) on CES follows the pseudo-second-order kinetic equation. The two different results obtained from R^2 values and error analysis values show the importance of error analysis while selecting a model.

Adsorption of As(III) and As(V) on CES follows the pseudo-second-order kinetic equation, indicating that two reactions occur simultaneously in the adsorption process, as assumed by the pseudo-second-order kinetic model. One

Table 5
Kinetic parameters of four kinetic equations with error analysis values

Adsorption kinetics	Parameters	Adsorbent for As(III)		Adsorbent for As(V)	
		ES	CES	ES	CES
Pseudo-first-order	k_1	0.037	0.038	0.036	0.042
	q_e (calculated from equation)	0.874	0.916	0.187	0.280
	q_e (experiment)	0.208	0.217	0.218	0.247
	R^2	0.911	0.917	0.908	0.975
	χ^2	3.715	3.894	0.033	0.072
	RMSE	0.661	0.693	0.027	0.043
	APE (%)	447.455	442.767	13.703	25.110
	SNE	3.000	3.000	1.404	3.000
Pseudo-second-order	q_e (calculated from equation)	0.349	0.355	0.264	0.294
	q_e (experiment)	0.208	0.217	0.218	0.247
	k_2	0.024	0.025	0.164	0.114
	$h = k_2 q_e^2$	0.003	0.003	0.008	0.010
	R^2	0.950	0.968	**0.980**	**0.983**
	χ^2	0.006	**0.0043**	0.153	**0.012**
	RMSE	**0.0122**	**0.011**	0.044	**0.016**
	APE (%)	6.458	4.880	23.889	**8.232**
	SNE	0.034	**0.028**	3.000	**0.877**
Elovich equation	α	0.092	0.094	0.066	0.072
	β	11.890	11.574	16.155	14.947
	R^2	**0.971**	**0.980**	0.892	0.882
	χ^2	**0.005**	0.0045	**0.017**	0.020
	RMSE	0.0123	0.012	**0.020**	0.023
	APE (%)	**5.793**	**4.419**	**10.557**	10.662
	SNE	**0.033**	0.029	**1.012**	1.232
Weber and Morris Intraparticle Diffusion Model	k_{int}	0.017	0.017	0.014	0.013
	c	–0.015	–0.011	0.049	0.083
	R^2	0.937	0.946	0.795	0.739
	χ^2	0.012	0.011	0.034	0.037
	RMSE	0.018	0.018	0.027	0.029
	APE (%)	9.412	7.965	15.157	14.850
	SNE	0.052	0.048	1.485	1.789

Highest R^2 value and the lowest χ^2, RMSE, APE (%), and SNE values among three kinetic models are in bold.

Table 6
Comparison of optimum conditions and isotherm constants of arsenic adsorption with other studies

Adsorbents	Optimum conditions	Removal percentage/ adsorption capacity	Langmuir		Freundlich		References
			b (L/mg)	Q_0 (mg/g)	k_f	n	
		As(III) adsorption					
Eggshell	Initial concentration (mg/L): 2; adsorbent dose (g/L):	64.98%	0.955	0.581	0.269	2.78	This study
Eggshell carbonized at 700°C	6; pH: 7; contact time (h): 2.67	65.28%	0.933	0.591	0.275	2.78	
Basic oxygen furnace slag (steel industry)	Initial concentration (mg/L): 1; adsorbent dose (g/L): 10; pH: 7; contact time (h): 12	99.9%	1.10	1.40	0.502	1.71	[21]
Pomegranate peel ($FeCl_3$ treated)	Initial concentration (mg/L): 20; adsorbent dose (g/L): 1; pH: 9; contact time (h): 2	70.7%	0.873	50	2.51	1.79	[27]
Fish scale	Initial concentration (mg/L): 0.5; adsorbent dose (g/L): 10; pH: 6.8; contact time (h): 130	83%	5.2	0.025	0.685	1.64	[26]
Siderite	Initial concentration (mg/L): 1; adsorbent dose (g/L): 20; contact time (h): 3	1.04 mg/g	1.9	1.040	0.013	0.59	[18]
		As(V) adsorption					
Eggshell	Initial concentration (mg/L): 2; adsorbent dose (g/L):	65.69%	0.390	0.892	0.263	2.00	This Study
Eggshell carbonized at 700°C	6; pH: 7; contact time (h): 1.33	71.62%	0.649	0.793	0.316	2.44	
synthetic zeolites (H-MFI-90)	Initial concentration (mg/L): 10; adsorbent dose (g/L): 2; pH: 3.15; contact time (h): 1.6	34.80 mg/g	0.011	34.8	4.21	1.12	[17]
Siderite	Initial concentration (mg/L): 1; adsorbent dose (g/L): 20; contact time (h): 3	0.52 mg/g	6.6	0.516	0.064	0.28	[18]
Orange peel	Initial concentration (mg/L): 10; adsorbent dose (g/L): 10; pH: 7; contact time(h): 2	4.7 mg/g	-	-	0.42	0.72	[56]
Oat hulls	Initial concentration (mg/L): 0.25; adsorbent dose (g/L): 0.015; pH: 5; contact time (h): 24	58%	-	2.04	0.42	2.48	[57]
Fish scale	Initial concentration (mg/L): 0.33; adsorbent dose (g/L): 10; pH: 6.8; contact time (h): 130	94%	8.8	0.027	0.396	1.54	[26]

of the reactions occurs at a faster rate and reaches equilibrium quickly while the other reaction occurs at a slow rate and continues during the adsorption process. Moreover, the adsorption process is controlled by the chemisorption process [55]. As adsorption of As(III) and As(V) on ES follows the Elovich kinetic equation, this also suggests that the adsorption process is a chemisorption process [34]. However, the adsorption rate on ES decreases exponentially with an increase in the quantity of adsorbed ions, as described by the model. Furthermore, the intraparticle diffusion model suggests that both the surface adsorption and the intraparticle diffusion occurred during the process of adsorption, as the graph obtained is not linear as shown in Fig. 13d. The first linear portion represents the instantaneous adsorption on the outer surface, and the second portion depicts mesopore/micropore diffusion [49].

3.5. Comparison of adsorption capacity of adsorbents with previous studies

Table 6 shows a comparison of the optimum conditions obtained for the removal of arsenic along with a comparison of the isotherm constants with previous studies. Comparing the removal efficiency of the adsorbents used in this study with previously studied adsorbents, it is found that these adsorbents are less efficient than the other adsorbents. However, we observe that the conditions of the removal are unfavorable for drinking water treatment. The adsorbents are toxic, or toxic after chemical treatment, or they are not removed in neutral pH, or they have very high contact time. In addition, when we compare the isotherm constants, the value of n of the adsorbents used in this study is >2, representing good adsorption. However, most of the adsorbents used previously have a value of n of <2, representing moderately difficult adsorption. Taking the optimum conditions into consideration, the adsorbents used in this study are better adsorbents than the other adsorbents, to treat groundwater. Hence, it is encouraging to use a locally available, non-toxic waste material for the treatment of arsenic-contaminated water.

4. Conclusions

The use of eggshell, a waste product, has been studied for arsenite and arsenate removal. The arsenic removal capacity of eggshell is found to be significant, and it is a nontoxic waste material that can be used suitably to treat drinking water. FTIR spectra showed that the distinct functional group present in ES and CES is the carbonate group (due to the presence of calcium carbonate) and is responsible for adsorption. The BET surface area of ES and CES is 0.78 and 0.44 m^2/g, respectively, and they contain mesopores. SEM images revealed that the adsorbents are composed of particles with smooth surfaces. As(III) and As(V) adsorption increased with increasing dose and contact time and was highly dependent on the pH of the solution. Favorable adsorption took place with 6 g/L of adsorbent dose, at pH 9 and 6 for As(III) and As(V), respectively. The point of zero charge for ES was at pH 8.03. As(V) was removed in a time of 80 min, as compared with the As(III) equilibrium time of 160 min. Under these conditions, ES and CES removed 68.54% and 70.09% of As(III) ions, respectively. Similarly, ES and CES removed 72.01% and 76.44% of As(V) ions, respectively. Moreover, removal efficiency is significant at neutral pH. However, the presence of competing ions, such as phosphate and nitrate, reduced the arsenic removal efficiency, drastically. The best isotherm to describe As(III) uptake is the Langmuir isotherm, revealing monolayer adsorption. The best isotherm to describe As(V) uptake is the Freundlich isotherm, revealing multilayer adsorption. Experimental kinetic model data fit the pseudo-second-order kinetic equation for adsorption of As(III) and As(V) on CES. Similarly, kinetic model data fit the Elovich kinetic equation for adsorption of As(III) and As(V) on ES. The kinetic model concluded that the adsorption process occurs through the chemisorption process. This result is also supported by FTIR and EDX results where it was shown that the presence of $CaCO_3$ in eggshell is the major reason for the adsorption of arsenic. Furthermore, the study of the intraparticle diffusion model confirmed the presence of both surface adsorption and the intraparticle diffusion mechanism during adsorption of arsenic. The goodness of fit of isotherm and kinetic models was studied by using three different error analysis tools. It was concluded that the goodness of fit of a model, based only on the R^2 value, is not enough. Further studies are suggested for the investigation of adsorption capacity at various temperatures and to carry out thermodynamic studies, including the activation energy, enthalpy, and entropy of activation.

Symbols

q_e	—	Amount of arsenic uptake per gram of adsorbent at equilibrium, mg/g
V	—	Volume of solution, L
M	—	Mass of adsorbent, g
C_i	—	Initial arsenic concentration, mg/L
C_e	—	Equilibrium arsenic concentration, mg/L
b	—	Langmuir constant, indicating adsorption rate, L/mg
Q_0	—	Langmuir constant, indicating monolayer adsorption capacity, mg/g
R_L	—	Separation factor
k_f	—	Freundlich constant, indicating the adsorption capacity
k_{int}	—	Intraparticle diffusion rate constant, $mgg^{-1}min^{-0.5}$
n	—	Freundlich constant, indicating the adsorption intensity
K_e	—	Elovich equilibrium constant, L/mg
q_m	—	Elovich maximum adsorption capacity, mg/g
k_1	—	pseudo-first-order rate coefficient, min^{-1}
q_t	—	Amount of arsenic adsorbed per gram of adsorbent at any time, mg/g
k_2	—	pseudo-second-order rate constant
α	—	Initial sorption rate, mg/g min
β	—	Desorption constant, g/mg
χ^2	—	Chi-Square
$q_{e,exp}$	—	Adsorption capacity, obtained from experiment, mg/g
$q_{e,cal}$	—	Adsorption capacity, obtained from theoretical calculation using the model, mg/g
N	—	Number of observations

Acknowledgments

The first author would like to thank the Sirindhorn International Institute of Technology (SIIT) for an Excellent Foreign Student (EFS) (graduate student) scholarship. The authors also thank SIIT for supporting the laboratory and financial budget to complete this work.

References

[1] G.S. Murugesan, M. Sathishkumar, K. Swaminathan, Arsenic removal from groundwater by pretreated waste tea fungal biomass, Bioresour. Technol., 97 (2006) 483–487.
[2] M.A. Rehman, I. Yusoff, R. Ahmmad, Y. Alias, Arsenic adsorption using palm oil waste clinker sand biotechnology: an experimental and optimization approach, Water Air Soil Pollut., 226 (2015) 149.
[3] R. Singh, S. Singh, P. Parihar, V.P. Singh, S.M. Prasad, Arsenic contamination, consequences and remediation techniques: a review, Ecotoxicol. Environ. Saf., 112 (2015) 247–270.
[4] WHO, Guidelines for Drinking-water Quality, Volume 1: Recommendations, 4th ed., World Health Organization, Geneva, 2011.
[5] C.O. Abernathy, Y.-P. Liu, D. Longfellow, H.V. Aposhian, B. Beck, B. Fowler, Arsenic: health effects, mechanisms of actions, and research issues, Environ. Health Perspect., 107 (1999) 593–597.
[6] J. Joshi, O. Sahu, Protection of human health by low cost treatment in rural area, J. Med. Eng. Technol., 2 (2014) 5–9.
[7] P. Bhattacharya, A.H. Welch, K.G. Stollenwerk, M.J. McLaughlin, J. Bundschuh, G. Panaullah, Arsenic in the environment: biology and chemistry, Sci. Total Environ., 379 (2007) 109–120.
[8] B. Mueller, Preliminary trace element analysis of arsenic in Nepalese groundwater may pinpoint its origin, Environ. Earth Sci., 77 (2018) 35–40.
[9] D. Chatterjee, M. Mazumder, S. Barman, J. Adhikari, A.K. Kundu, A. Mukherjee, A. Das, P. Ghosh, U. Mandal, D. Chatterjee, Arsenic in Groundwater: Distribution and Geochemistry in Nadia District, West Bengal, India, A. Mukherjee, Ed., Groundwater of South Asia, Springer Hydrogeology, Springer, Singapore, 2018, pp. 349–373.
[10] A. Rasool, T. Xiao, A. Farooqi, M. Shafeeque, Y. Liu, M.A. Kamran, Quality of tube well water intended for irrigation and human consumption with special emphasis on arsenic contamination at the area of Punjab, Pakistan, Environ. Geochem. Health, 39 (2017) 847–863.
[11] R. Li, Y.-M. Kuo, W.-w. Liu, C.-S. Jang, E. Zhao, L. Yao, Potential health risk assessment through ingestion and dermal contact arsenic-contaminated groundwater in Jianghan plain, China, Environ. Geochem. Health, 40 (2018), 1585–1599.
[12] M.E. Huq, C. Su, S. Fahad, J. Li, M.S. Sarven, R. Liu, Distribution and hydrogeochemical behavior of arsenic enriched groundwater in the sedimentary aquifer comparison between Datong basin (China) and Kushtia district (Bangladesh), Environ. Sci. Pollut. Res., 25 (2018), 15830–15843.
[13] T. Rujiralai, N. Juansai, W. Cheewasedtham, Arsenic determination in soils and hair from schools in past mining activity areas in Ron Phibun district, Nakhon Si Thammarat province, Thailand and relationship between soil and hair arsenic, Chem. Pap., 72 (2018), 381–391.
[14] V.M. Marín-Rangel, R. Cortés-Martínez, R.A. Cuevas Villanueva, M. Garnica-Romo, H.E. Martínez-Flores, As (V) biosorption in an aqueous solution using chemically treated lemon (*Citrus aurantifolia* swingle) residues, J. Food Sci., 77 (2012), T10–T14.
[15] S.R. Kanel, J.-M. Greneche, H. Choi, Arsenic (V) removal from groundwater using nano scale zero-valent iron as a colloidal reactive barrier material, Environ. Sci. Technol., 40 (2006), 2045–2050.
[16] J.G. Hering, P.-Y. Chen, J.A. Wilkie, M. Elimelech, Arsenic removal from drinking water during coagulation, J. Environ. Eng., 123 (1997), 800–807.
[17] P. Chutia, S. Kato, T. Kojima, S. Satokawa, Arsenic adsorption from aqueous solution on synthetic zeolites, J. Hazard. Mater., 162 (2009), 440–447.
[18] H. Guo, D. Stüben, Z. Berner, Adsorption of arsenic (III) and arsenic (V) from groundwater using natural siderite as the adsorbent, J. Colloid Interface Sci., 315 (2007), 47–53.
[19] D. Dickson, G. Liu, Y. Cai, Adsorption kinetics and isotherms of arsenite and arsenate on hematite nanoparticles and aggregates, J. Environ. Manage., 186 (2017), 261–267.
[20] S. De Gisi, G. Lofrano, M. Grassi, M. Notarnicola, Characteristics and adsorption capacities of low-cost sorbents for wastewater treatment: a review, Sustainable Mater. Technol., 9 (2016), 10–40.
[21] S. Kanel, H. Choi, Removal of arsenic from groundwater by industrial byproducts and its comparison with zero-valent iron, J. Hazard. Toxic Radioact. Waste, 21 (2016), 04016028.
[22] D. Mohan, C.U. Pittman, Arsenic removal from water/wastewater using adsorbents—a critical review, J. Hazard. Mater., 142 (2007), 1–53.
[23] G. Manju, C. Raji, T. Anirudhan, Evaluation of coconut husk carbon for the removal of arsenic from water, Water Res., 32 (1998), 3062–3070.
[24] Y. Tian, M. Wu, X. Lin, P. Huang, Y. Huang, Synthesis of magnetic wheat straw for arsenic adsorption, J. Hazard. Mater., 193 (2011), 10–16.
[25] M. Sidhu, P. Sama, J. Parmar, S.M. Bhatt, Biosorption of arsenic (III) from drinking water by using low cost biosorbents derived from peels of oranges, turnip and peanut shells, Int. J. Pharm. Res. Drug Dev., 1 (2014), 66–69.
[26] M. Rahaman, A. Basu, M. Islam, The removal of As (III) and As (V) from aqueous solutions by waste materials, Bioresour. Technol., 99 (2008), 2815–2823.
[27] S. Thapa, M.R. Pokhrel, Removal of As (III) from aqueous solution using Fe (III) loaded pomegranate waste, J. Nepal Chem. Soc., 30 (2013), 29–36.
[28] Z. Wei, C. Xu, B. Li, Application of waste eggshell as low-cost solid catalyst for biodiesel production, Bioresour. Technol., 100 (2009), 2883–2885.
[29] M. Pettinato, S. Chakraborty, H.A. Arafat, V. Calabro, Eggshell: a green adsorbent for heavy metal removal in an MBR system, Ecotoxicol. Environ. Saf., 121 (2015), 57–62.
[30] J.A Otun, I.A. Oke, N.O. Olarinoye, D.B. Adie, C.A. Okuofu, Adsorption isotherms of Pb (II), Ni (II) and Cd (II) ions onto PES, J. Appl. Sci., 6 (2006), 2368–2376.
[31] WEF, APHA, Standard Methods for the Examination of Water and Wastewater, W.E. Federation, American Public Health Association, Washington, DC, USA, 2005.
[32] P. Smedley, D. Kinniburgh, A review of the source, behaviour and distribution of arsenic in natural waters, Appl. Geochem., 17 (2002), 517–568.
[33] K. Foo, B.H. Hameed, Insights into the modeling of adsorption isotherm systems, Chem. Eng. J., 156 (2010), 2–10.
[34] K.U. Ahamad, R. Singh, I. Baruah, H. Choudhury, M.R. Sharma, Equilibrium and kinetics modeling of fluoride adsorption onto activated alumina, alum and brick powder, Groundwater Sustainable Dev., 7 (2018) 452–458.
[35] S. Eris, S. Azizian, Analysis of adsorption kinetics at solid/solution interface using a hyperbolic tangent model, J. Mol. Liq., 231 (2017), 523–527.
[36] M. Iqbal, A. Saeed, S.I. Zafar, FTIR spectrophotometry, kinetics and adsorption isotherms modeling, ion exchange, and EDX analysis for understanding the mechanism of Cd^{2+} and Pb^{2+} removal by mango peel waste, J. Hazard. Mater., 164 (2009), 161–171.
[37] M.I. El-Khaiary, G.F. Malash, Y.-S. Ho, On the use of linearized pseudo-second-order kinetic equations for modeling adsorption systems, Desalination, 257 (2010), 93–101.
[38] H. Qiu, L. Lv, B.-C. Pan, Q.-J. Zhang, W.-m. Zhang, Q.-X. Zhang, Critical review in adsorption kinetic models, J. Zhejiang Univ. Sci. A, 10 (2009), 716–724.
[39] Z. Harrache, M. Abbas, T. Aksil, M. Trari, Thermodynamic and kinetics studies on adsorption of Indigo Carmine from aqueous solution by activated carbon, Microchem. J., 144 (2019), 180–189.

[40] M.I. El-Khaiary, G.F. Malash, Common data analysis errors in batch adsorption studies, Hydrometallurgy, 105 (2011), 314–320.
[41] M. Thommes, K. Kaneko, A.V. Neimark, J.P. Olivier, F. Rodriguez-Reinoso, J. Rouquerol, K.S.W. Sing, Physisorption of gases, with special reference to the evaluation of surface area and pore size distribution (IUPAC Technical Report), Pure Appl. Chem., 87 (2015), 1051–1069.
[42] P.D. Pathak, S.A. Mandavgane, B.D. Kulkarni, Characterizing fruit and vegetable peels as bioadsorbents, Curr. Sci., 110 (2016), 00113891.
[43] W. Tsai, J. Yang, C. Lai, Y. Cheng, C. Lin, C. Yeh, Characterization and adsorption properties of eggshells and eggshell membrane, Bioresour. Technol., 97 (2006), 488–493.
[44] J.V. Flores-Cano, R. Leyva-Ramos, J. Mendoza-Barron, R.M. Guerrero-Coronado, A. Aragón-Piña, G.J. Labrada-Delgado, Sorption mechanism of Cd (II) from water solution onto chicken eggshell, Appl. Surf. Sci., 276 (2013), 682–690.
[45] S. Lunge, D. Thakre, S. Kamble, N. Labhsetwar, S. Rayalu, Alumina supported carbon composite material with exceptionally high defluoridation property from eggshell waste, J. Hazard. Mater., 237 (2012), 161–169.
[46] P.D. Pathak, S.A. Mandavgane, Preparation and characterization of raw and carbon from banana peel by microwave activation: application in citric acid adsorption, J. Environ. Chem. Eng., 3 (2015), 2435–2447.
[47] S.R. Kanel, H. Choi, J.-Y. Kim, S. Vigneswaran, W.G. Shim, Removal of arsenic (III) from groundwater using low-cost industrial by-products-blast furnace slag, Water Qual. Res. J., 41 (2006), 130–139.
[48] G. Annadurai, R.S. Juang, D.J. Lee, Adsorption of heavy metals from water using banana and orange peels, Water Sci. Technol., 47 (2003), 185–190.
[49] X. Liu, H. Ao, X. Xiong, J. Xiao, J. Liu, Arsenic removal from water by iron-modified bamboo charcoal, Water Air Soil Pollut., 223 (2012), 1033–1044.
[50] P.V. Brady, J.V. Walther, Surface chemistry and silicate dissolution at elevated temperatures, Am. J. Sci., 292 (1992), 639–658.
[51] Y. Jeong, F.A.N. Maohong, J. Van Leeuwen, J.F. Belczyk, Effect of competing solutes on arsenic (V) adsorption using iron and aluminum oxides, J. Environ. Sci., 19 (2007), 910–919.
[52] S.R. Kanel, B. Manning, L. Charlet, H. Choi, Removal of arsenic (III) from groundwater by nanoscale zero-valent iron, Environ. Sci. Technol., 39 (2005), 1291–1298.
[53] T. Motsi, N. Rowson, M. Simmons, Adsorption of heavy metals from acid mine drainage by natural zeolite, Int. J. Miner. Process., 92 (2009), 42–48.
[54] J. Anwar, U. Shafique, M. Salman, A. Dar, S. Anwar, Removal of Pb (II) and Cd (II) from water by adsorption on peels of banana, Bioresour. Technol., 101 (2010), 1752–1755.
[55] P. Satish, R. Sameer, P. Naseema, Defluoridation of water using biosorbents: kinetic and thermodynamic study, Int. J. Res. Chem. Environ., 3 (2013), 125–135.
[56] M.I. Khaskheli, S.Q. Memon, A.N. Siyal, M.Y. Khuhawar, Use of orange peel waste for arsenic remediation of drinking water, Waste Biomass Valorization, 2 (2011), 423–433.
[57] C. Chuang, M. Fan, M. Xu, R. Brown, S. Sung, B. Saha, Adsorption of arsenic (V) by activated carbon prepared from oat hulls, Chemosphere, 61 (2005), 478–483.